Primary Tumors of the Pituitary Gland: Radiologic-Pathologic Correlation

Robert Y. Shih, MD
Jason W. Schroeder, MD
Kelly K. Koeller, MD

Abbreviations: ACP = adamantinomatous craniopharyngioma, ACTH = adrenocorticotropic hormone, CNS = central nervous system, H-E = hematoxylin-eosin, PCP = papillary craniopharyngioma, RCC = Rathke cleft cyst

RadioGraphics 2021; 41:2029–2046

https://doi.org/10.1148/rg.2021200203

Content Codes: CT MR NR

From the Department of Radiology, Uniformed Services University of the Health Sciences, 4301 Jones Bridge Rd, Bethesda, MD 20814 (R.Y.S.); Department of Radiology, Walter Reed National Military Medical Center, Bethesda, Md (J.W.S.); and Department of Radiology, Mayo Clinic, Rochester, Minn (K.K.K.). Received October 30, 2020; revision requested May 11, 2021, and received June 6; accepted June 10. For this journal-based SA-CME activity, the author K.K.K. has provided disclosures (see end of article); all other authors, the editor, and the reviewers have disclosed no relevant relationships. **Address correspondence to** R.Y.S. (e-mail: *robert.shih@usuhs.edu*).

The views expressed in this article are those of the authors and do not reflect the official policy of the Department of Defense or U.S. Government.

SA-CME LEARNING OBJECTIVES

After completing this journal-based SA-CME activity, participants will be able to:

- Recognize the various subtypes and imaging features of pituitary adenoma, which is the most common tumor of the adenohypophysis and the second most common primary tumor of the CNS.
- Understand the relationship between adenohypophyseal development from the stomodeum and the two histologic subtypes of craniopharyngioma, adamantinomatous and (squamous) papillary.
- Describe three rare neoplastic entities that can arise from specialized glial cells (pituicytes) in the neurohypophysis and infundibulum, which are an embryologic undergrowth of the diencephalon.

See rsna.org/learning-center-rg.

Primary tumors of the pituitary gland are the second most common histologic category of primary central nervous system tumors across all age groups and are the most common in adolescents to young adults, despite originating from a diminutive endocrine gland that is often described as "about the size of a pea." The vast majority of these represent primary tumors of the adenohypophysis, specifically pituitary adenomas, which can be either functional or silent with regard to hormone hypersecretion. According to the fourth edition of the World Health Organization classification of endocrine tumors, published in 2017, cellular lineage and immunohistochemical stains for pituitary hormones and/or transcription factors help with making the correct pathologic diagnosis. From a radiologic standpoint, microadenomas pose challenges for accurate detection and avoiding false-negative or false-positive results, while macroadenomas pose challenges from local mass effect on surrounding structures. Pituitary carcinoma and pituitary blastoma also arise from the adenohypophysis and are characterized by metastatic disease and infantile presentation, respectively. While primary tumors of the adenohypophysis are common, a second category comprising primary tumors of Rathke pouch (ie, craniopharyngioma) are uncommon, and a third category comprising primary tumors of the neurohypophysis (eg, pituicytoma) are rare. The authors review all three categories of pituitary tumors, with emphasis on radiologic-pathologic correlation, including the typical neuroimaging, histologic, and molecular features that may point toward a specific diagnosis.

Introduction

According to the Central Brain Tumor Registry of the United States, which collected over 400 000 diagnoses of primary central nervous system (CNS) tumors in the 5-year period 2012–2016, tumors of the pituitary gland were the second most frequently reported histology (16.8%), following meningioma (37.6%) and followed by glioblastoma (14.6%) (1). In a separate analysis of primary CNS tumors specifically in adolescents and young adults (age, 15–39 years), tumors of the pituitary were the most common histologic category (29.9%), followed by meningioma (15.9%) and astrocytoma (15.3%) (2). These epidemiologic statistics are impressive for a diminutive endocrine gland that is often described as "about the size of a pea," generally measuring less than 1 cm and weighing less than 1 g in the adult human. From within the saddle-shaped sella turcica of the sphenoid bone, this tiny "master gland of the body" secretes a total of eight hormones and directs multiple processes of growth, homeostasis, and reproduction (3).

The name *pituitary* is derived from a misunderstanding by early anatomists, who thought it played a role in nasal mucus secretion (*pituita* means phlegm). The more accurate but less popular alternative

TEACHING POINTS

- Only the posterior pituitary gland (neurohypophysis) is an embryogenetic undergrowth from the hypothalamus or diencephalon; the anterior pituitary gland (adenohypophysis) is formed not from neuroectoderm but by a diverticulum of oral ectoderm from the primitive mouth or stomodeum. This outpouching, first described by German embryologist Martin Heinrich Rathke in 1839, is known as Rathke pouch.
- Pituitary adenomas typically show delayed enhancement and washout relative to that of a normal gland on postcontrast images. An additional dynamic postcontrast sequence can sometimes be helpful for accentuating differential enhancement and delineating tumor, such as in the setting of clinically suspected microadenoma.
- Because of their larger size, macroadenomas are easier to identify at cross-sectional imaging. Aside from an expanded pituitary contour, displacement of the infundibulum and suprasellar extension are common, with optic chiasm and/or nerve compression, cavernous sinus invasion, and erosion of the sellar margin seen in larger tumors. The Hardy and Knosp classification systems have been used to quantitate the degree of invasion into the sella and parasellar regions by these macroadenomas.
- Craniopharyngioma is uncommon, with an incidence of 0.13 per 100 000 person-years, and the age distribution will vary depending on the subtype. ACPs account for 90% of craniopharyngiomas, while (squamous) PCPs represent the remaining 10%. While PCP is nearly always found in adults, ACP has a bimodal distribution, peaking in children younger than 18 years of age and in adults 40–60 years of age.
- While SCO was initially thought to arise from nonendocrine folliculostellate cells within the anterior pituitary gland, these three entities are now all thought to arise from specialized glial cells (pituicytes) within the posterior pituitary gland: "pituicytomas, granular cell tumors of the sellar region and spindle cell oncocytomas show nuclear expression of thyroid transcription factor 1 (TTF-1), suggesting that these three tumors may constitute a spectrum of a single neurological entity."

term is *hypophysis*, which is derived from the Greek word for undergrowth and describes its anatomic relationship with the hypothalamus, which regulates its function. As it turns out, only the posterior pituitary gland (neurohypophysis) is an embryogenetic undergrowth from the hypothalamus or diencephalon; the anterior pituitary gland (adenohypophysis) is formed not from neuroectoderm but by a diverticulum of oral ectoderm from the primitive mouth or stomodeum (Fig 1). This outpouching, first described by German embryologist Martin Heinrich Rathke in 1839, is known as Rathke pouch. Alternatively, it is also known as the craniopharyngeal duct because of its course from the oral cavity to the pharynx through the sphenoid body into the cranial vault. Whereas the posterior pituitary gland has direct axonal projections from the hypothalamus through the infundibulum, the anterior pituitary gland receives hypothalamic signaling through the vascular hypophyseal portal system (3).

This developmental background structures our discussion on primary tumors of the pituitary gland into three sections, which are ordered from most common to least common: primary tumors of the adenohypophysis, primary tumors of Rathke pouch (embryonic precursor of the adenohypophysis), and primary tumors of the neurohypophysis (Table).

Primary Tumors of Adenohypophysis

The prefix *adeno-* reflects the differentiation of Rathke pouch into glandular epithelium, which synthesizes, stores, and secretes six endocrine hormones. Pituitary adenomas are monoclonal tumors arising from the adenohypophysis and are the most common neuroendocrine tumors of the pituitary gland (4). The true incidence is uncertain, with recent population-based studies showing a prevalence of clinically significant adenomas ranging from 1:865 to 1:2688 (5). Most pituitary adenomas are incidental without clinical significance (6). Pituitary adenomas smaller than 10 mm are called microadenomas, while those 10 mm or larger are called macroadenomas, and the term *giant pituitary adenoma* has been used to describe tumors 40 mm or larger in maximum diameter (4).

While the vast majority (~95%) of pituitary adenomas occur sporadically, about 5% arise in familial or hereditary conditions (6–8). In autosomal dominant multiple endocrine neoplasia 1 (MEN 1), pituitary tumors tend to occur earlier; are more aggressive, invasive, and resistant to therapy; and have higher rates of recurrence (4). Familial isolated pituitary adenoma (FIPA) is an autosomal dominant condition with mutations in the *AIP* gene that encodes aryl-hydrocarbon receptor–interacting protein, usually manifesting with invasive macroadenomas during childhood or young adulthood (4). Rarely, pituitary adenoma may occur with paraganglioma and pheochromocytoma, related to a mutation affecting succinate dehydrogenase (9). Other associated genetic conditions include McCune-Albright syndrome, Carney complex, and X-linked acrogigantism (6,7).

Clinical Presentation

Pituitary adenomas that secrete excess hormones are considered functional adenomas and account for two-thirds of clinically evident adenomas (5–7). As a general rule, women tend to present with symptoms earlier in life, often being diagnosed with a prolactin-secreting adenoma, while men tend to present with symptoms later in life, often being diagnosed with a nonfunctional or nonsecretory macroadenoma (10). Macroadenomas can result in headache and visual field deficits related to local mass effect and extension

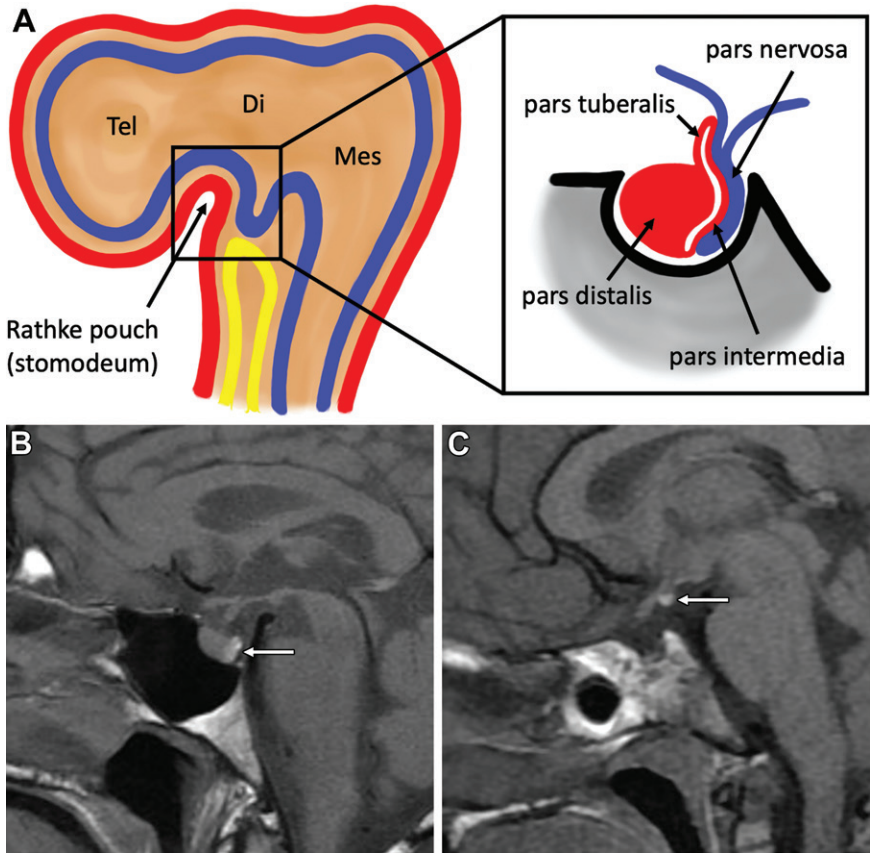

Figure 1. Anatomy and development of the pituitary gland. **(A)** Schematic diagram shows the dual embryologic origin of the pituitary gland. The anterior pituitary gland or adenohypophysis derives from an upward diverticulum (Rathke pouch) of the surface ectoderm (red line) from the primitive mouth or stomodeum. In contrast, the pituitary infundibulum and posterior pituitary gland or neurohypophysis derive from a downward diverticulum of the neuroectoderm (blue line) from the diencephalon *(Di)*. These differences in origin are reflected in the histologies and locations for primary tumors of the pituitary gland. *Mes* = mesencephalon, *Tel* = telencephalon, yellow line = endoderm. **(B)** Sagittal T1-weighted MR image shows a normally developed pituitary gland in a young adult with an isointense adenohypophysis (80%) versus hyperintense neurohypophysis (arrow) due to high protein content. The adenohypophysis and funnel-shaped infundibulum are both expected to enhance owing to a rich vascular hypophyseal portal system (endocrine function). The optic chiasm and third ventricle are located superiorly. **(C)** Sagittal T1-weighted MR image shows an abnormally developed pituitary gland in a young child with growth retardation due to pituitary stalk interruption syndrome. Failure of a downward diverticulum from the diencephalon has resulted in an ectopic position of the posterior pituitary bright spot (arrow), absence of the pituitary stalk (infundibulum), and marked hypoplasia of the anterior pituitary in the sella turcica due to disconnection from the hypothalamus. Patients with these findings are diagnosed with severe growth hormone deficiency.

into the suprasellar region with optic chiasm and/or nerve compression. Lateral cavernous sinus invasion can cause cranial nerve III, IV, or VI palsies. Compression of the pituitary gland or stalk (infundibulum) may cause hypopituitarism (11).

While these symptoms are usually chronic, pituitary apoplexy (from the Greek term *apoplexia* for stroke) is acute infarction or hemorrhage within the pituitary gland, occurring most commonly in preexisting macroadenomas. It is characterized by acute onset of symptoms, such as severe headache, visual loss, ophthalmoplegia, or endocrine dysfunction, all of which reflect sudden tumoral expansion. Predisposing factors include hypertension, pregnancy, major surgery, hypotension, dopamine agonist therapy, and anticoagulation therapy (12).

Pituitary tumors are classified by histopathologic results, cellular lineage, and immunohistochemical markers (Table). Among the clinically evident pituitary adenomas, lactotroph adenomas are most common (46%–66%), followed by nonfunctional adenomas (15%–37%), somatotroph adenomas (9%–17%), corticotroph adenomas (2%–6%), and thyrotroph adenomas (~1%) (5,6). Most pituitary adenomas are definitively classified by the results of hormone immunohistochemicial analysis (7). No biomarker has been identified that conclusively predicts the clinicopathologic behavior of an adenoma (4). In the following sections, we review different subtypes of pituitary adenoma, followed by two rare alternative neoplasms of the adenohypophysis: pituitary carcinoma and pituitary blastoma.

Lactotroph Adenoma (Prolactinoma)

Lactotroph adenoma is the most common functional pituitary adenoma and secretes prolactin. It often manifests as a microadenoma in the lateral and posterior portion of the anterior pituitary gland in young women (peak age, 20–40 years), but it can also manifest as a macroadenoma in men and children. Typical symptoms in women include galactorrhea and secondary amenorrhea, versus erectile dysfunction, decreased libido, hypopituitarism, or visual field defects in men, whereas delayed puberty and primary amenorrhea are frequently seen in children (8).

There is a correlation between the size of the tumor and the serum prolactin level. Levels of 100–250 ng/mL (4348–10 870 pmol/L) are typical for a microadenoma, while levels greater than 250

Primary Tumors of the Pituitary Gland with Typical Features

Category	Cells of Origin	Neoplasms*	Features
Primary tumors of adenohypophysis	Lactotroph (prolactin)	Pituitary microadenoma	May manifest clinically from hormonal excess or as benign incidental finding
	Somatotroph (GH)		
	Corticotroph (ACTH)	Pituitary macroadenoma	May manifest clinically from hormonal excess or mass effect on local structures
	Thyrotroph (TSH)		
	Gonadotroph (FSH/LH)		
	Pit-1 lineage (Pit-1)	Pituitary carcinoma	Same as adenoma plus extrasellar metastases
	"Null cell" (negative)		
	Undifferentiated or poorly differentiated adenohypophyseal cells	Pituitary blastoma	Pituitary mass in infant with Cushing syndrome
Primary tumors of Rathke pouch	Oral ectoderm	Rathke cleft cyst*	Nonneoplastic cyst without evidence of solid enhancement
		Adamantinomatous craniopharyngioma (β-catenin)	Mixed cystic-solid suprasellar mass with calcification in child or adult
		Papillary craniopharyngioma (VE1)	Mostly solid suprasellar mass in adult
Primary tumors of neurohypophysis	Pituicyte (TTF-1)	Pituicytoma	Solid enhancing mass in neurohypophysis or infundibulum
		Granular cell tumor	Solid enhancing mass in infundibulum
		Spindle cell oncocytoma	Infiltrative intrasellar-suprasellar mass

Note.—Usual positive immunohistochemical stains are in parentheses. ACTH = adrenocorticotropic hormone, FSH = follicle-stimulating hormone, GH = growth hormone, LH = luteinizing hormone, TSH = thyroid stimulating hormone, TTF-1 = thyroid transcription factor 1, VE1 = antibody to *BRAF* V600E mutation.
*Except Rathke cleft cyst, which is not a neoplasm.

ng/mL suggest a macroadenoma and levels greater than 10 000 ng/mL (434 780 pmol/L) are common in larger macroadenomas (>3 cm) (5,8). There are three histologic subtypes: sparsely granulated lactotroph adenoma (most common), densely granulated lactotroph adenoma, and acidophil stem cell lactotroph adenoma (8).

Lactotroph adenomas are amenable to pharmacotherapy using dopamine agonists (Fig 2), such as cabergoline (85%–90% effective) and bromocriptine (75% effective) (4,8). In sparsely granulated lactotroph adenomas, the response to bromocriptine may be quite striking, with a rapid reduction in serum prolactin levels (10). Failure to respond indicates a more aggressive adenoma and necessitates a change in dosage or medication, versus surgical resection with possible radiation therapy (4).

Somatotroph Adenoma (Somatotropinoma)

Somatotroph adenoma is the second most common functional pituitary adenoma and secretes growth hormone. It is involved in more than 95% of cases of gigantism or acromegaly and may occur at any age (mean age, 47 years), without gender predilection. Mammosomatotroph adenomas that cosecrete growth hormone and prolactin can manifest in young women with both acromegaly and amenorrhea and/or galactorrhea. Elevated serum growth hormone and insulin-like growth factor 1 levels can support a diagnosis of gigantism or acromegaly and would prompt evaluation for a somatotropinoma (13).

Most somatotroph adenomas manifest as a macroadenoma (Fig 3). The tumor subtype of densely granulated somatotroph adenoma (DGSA) tends to manifest as a microadenoma in older adults and is the most common cause of acromegaly, while sparsely granulated somatotroph adenoma (SGSA) tends to manifest as a macroadenoma in younger women. At imaging, DGSA tends to be more T2 hypointense, while SGSA tends to be more T2 hyperintense, with suprasellar or cavernous sinus invasion. DGSA is also more responsive to somatostatin analogs than is SGSA. If there is no evidence of an adenoma in a young patient with acromegaly, then X-linked acrogigantism should be suspected (13).

Surgery is curative in up to 90% of microadenomas, compared with only 50% of macroadenomas (4). Repeat surgery, treatment with long-

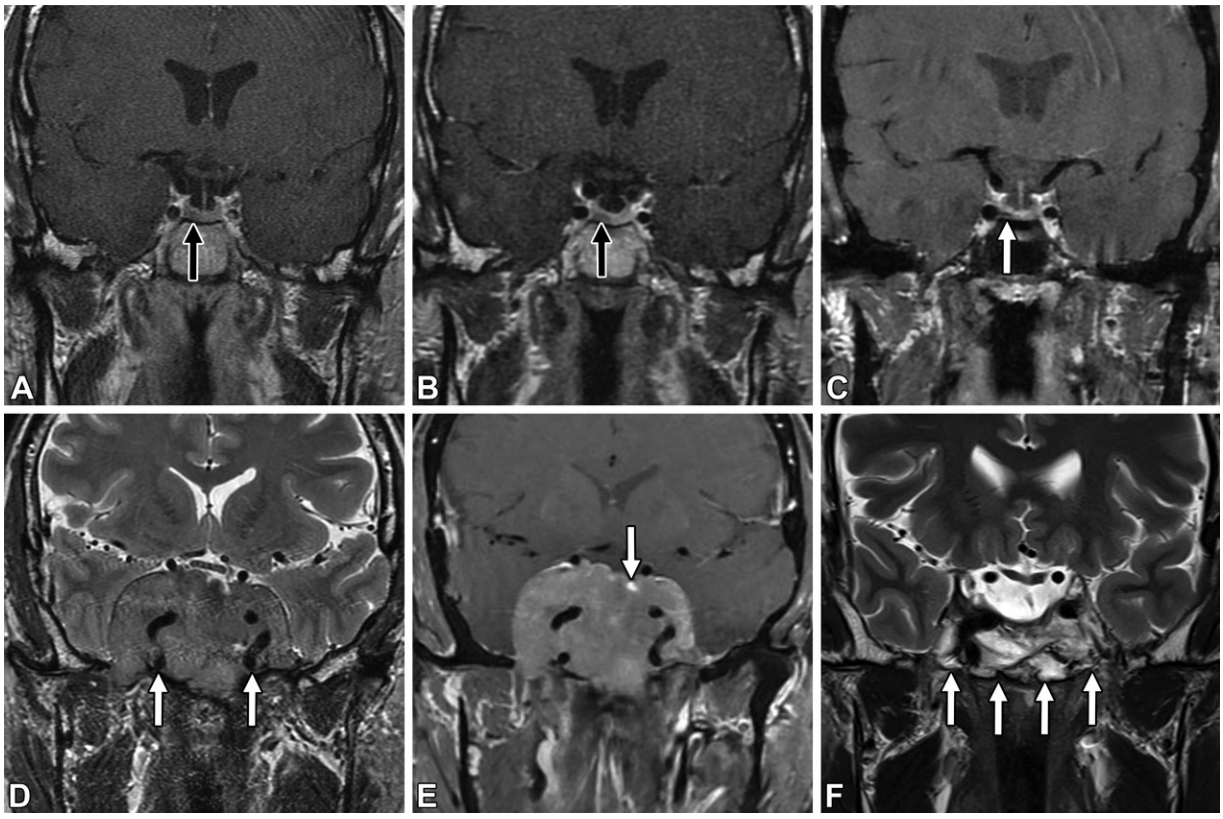

Figure 2. Lactotroph adenomas (prolactinomas). **(A)** Coronal contrast-enhanced T1-weighted MR image shows a subtle hypoenhancing lesion (arrow) in the right adenohypophysis in a middle-aged man with hyperprolactinemia, suspicious for a microadenoma. **(B)** Coronal dynamic contrast-enhanced T1-weighted MR image better shows delayed and differential enhancement of the right-sided lesion (arrow), increasing diagnostic confidence for microprolactinoma. **(C)** Coronal contrast-enhanced T1-weighted MR image after dopamine agonist therapy (cabergoline) shows significant interval decrease and regression in size of the right-sided lactotroph microadenoma (arrow). **(D)** Coronal T2-weighted MR image in another middle-aged man with severe hyperprolactinemia shows a large isointense mass centered around where the pituitary gland and sella turcica used to be. It invades the cavernous sinuses and encases the carotid arteries (arrows) but does not compress the optic chiasm. **(E)** Coronal contrast-enhanced T1-weighted MR image shows mild homogeneous enhancement of the giant macroadenoma (macroprolactinoma). A tiny amount of normal residual pituitary gland enhances much more intensely (arrow). Larger tumors can undergo cystic or hemorrhagic change, not seen in this case. **(F)** Coronal T2-weighted MR image after cabergoline therapy shows a significant decrease in tumor size and suprasellar-parasellar mass effect. There was also a gradual decrease in the serum prolactin level and an increase in T2 signal intensity (arrows), indicating successful treatment and decreased cellularity.

acting somatostatin analogs (such as octreotide or lanreotide), and radiation therapy may be needed to help achieve biochemical control (4,11). Some patients may have persistent hypersecretion in spite of tumor shrinkage (biochemical resistance) or vice versa (mass resistance) (4). Biochemically persistent SGSA may respond to pegvisomant, a growth hormone receptor antagonist (13).

Corticotroph Adenoma (Corticotropinoma)

Corticotroph adenoma is uncommon and secretes adrenocorticotropic hormone (ACTH) and other proopiomelanocortin-derived peptides. When the clinical presentation of Cushing syndrome is caused by a corticotropinoma, it is called Cushing disease, with a prevalence of three to 10 cases per 1 million, most common in women 30–50 years old. It is the most common adenoma (55%) in children under 11 years of age and is more common in boys. Most corticotroph adenomas (80%) show elevated serum ACTH and cortisol levels, but these features are absent in 20%, described as silent corticotroph adenomas (Fig 4) (14). Typical clinical manifestations of Cushing disease or syndrome include moon facies, buffalo hump, enlarging midsection, acne or striae, diabetes, and hypertension (5). A clinical diagnosis may be difficult owing to overlap with common conditions such as obesity, diabetes, and hypertension (14).

Most patients with Cushing disease (85%–90%) have a pituitary adenoma, while 10%–15% of cases are caused by an ectopic extrasellar adenoma (14,15). Most of these are microadenomas and tend to be affiliated with florid Cushing manifestations, while macroadenomas are associated with more cyclic or mild symptoms: "small tumor, big Cushing…big tumor, small Cushing" (10,14). Histopathologically, they are subdivided into densely granulated (usually

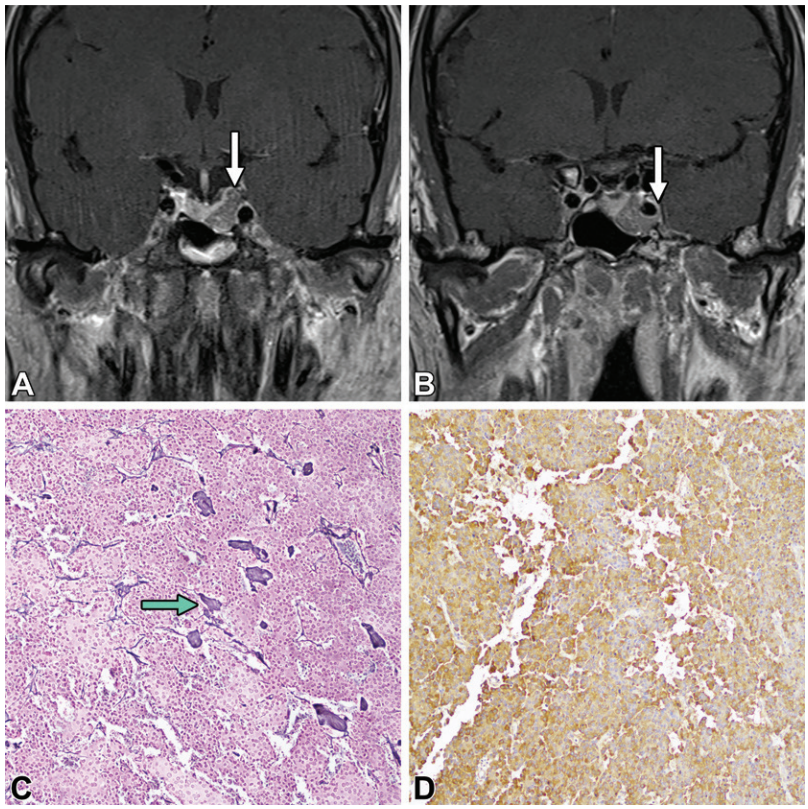

Figure 3. Somatotroph adenoma (somatotropinoma) in a middle-aged woman with headache and signs of acromegaly. **(A)** Coronal contrast-enhanced T1-weighted MR image shows a hypoenhancing mass, which is expanding the left lateral adenohypophysis (arrow). **(B)** More anterior coronal contrast-enhanced T1-weighted MR image from the same contrast-enhanced sequence as in **A** shows that the hypoenhancing mass wraps below the left cavernous carotid flow void and extends slightly past its lateral margin (arrow). It indicates probable invasion of the cavernous sinus (Knosp grade 3) and is relevant to surgical planning. **(C)** Low-power photomicrograph with reticulin stain shows numerous neuroendocrine cells with round nuclei. There is a distorted and fragmented reticulin staining pattern (arrow), which is consistent with loss of normal pituitary acinar architecture and confirms the diagnosis of a pituitary adenoma. **(D)** Low-power photomicrograph shows diffusely positive (brown) immunostaining for growth hormone, which correlates with the clinical history and confirms the diagnosis of somatotroph adenoma.

microadenomas), sparsely granulated, or Crooke cell adenomas (usually macroadenomas). Failure to localize a microcorticotropinoma with imaging is not uncommon (9%), even with 3-T MRI and inferior petrosal sinus sampling (14).

Without treatment, Cushing disease is lethal (14). Surgical resection of microadenomas can achieve remission in 60%–90% of patients (4). Lower cure rates are seen with macroadenomas (14). Pasireotide, a somatostatin analog, may be used to treat corticotroph adenomas that express somatostatin receptor protein type 5 (11). Bilateral adrenalectomy is another therapeutic option but will involve the risk of Nelson syndrome, with hyperpigmentation and muscle weakness (14).

Thyrotroph Adenoma (Thyrotropinoma)

Thyrotroph adenoma is rare and secretes thyroid-stimulating hormone. Like lactotroph and somatotroph adenomas, thyrotroph adenomas are derived from Pit-1 lineage adenohypophyseal cells, all of which will express pituitary-specific positive transcription factor 1. Elevated serum thyroid-stimulating hormone levels can result in clinical or biochemical thyrotoxicosis with elevated free thyroxine and triiodothyronine level. Most are macroadenomas with extrasellar extension. Pharmacotherapy (somatostatin analogs) for residual disease after surgical resection is efficacious in more than 90% of cases (16).

Silent versus Null Cell Adenoma

Silent adenomas show histopathologic and immunohistochemical features consistent with a specific cellular lineage but without clinical evidence of hormonal hypersecretion. They account for most cases of nonfunctional or nonsecretory pituitary adenoma. For example, most gonadotroph adenomas are clinically silent and are therefore identified during histopathologic analysis with immunostaining for follicle-stimulating hormone and luteinizing hormone, while silent lactotroph or somatotroph adenomas are relatively rare (7).

A pituitary adenoma without evidence of cell-specific differentiation by hormones, transcription factors, or other immunomarkers (hormone immunonegative) is defined as a "null cell" adenoma and accounts for less than 5% of clinically nonfunctional adenomas (7,17). Because of the absence of hormone secretion, it tends to manifest in older adults as a macroadenoma, often with extrasellar extension. The prognosis is good if completely resected, with radiation therapy reserved for residual disease (17).

Plurihormonal versus Double Adenoma

Plurihormonal adenoma (~1% of all pituitary adenomas) is a tumor secreting multiple hormones. It can be monomorphous (derived from a single cell line) or plurimorphous (derived from multiple distinct cell lines). On the other hand,

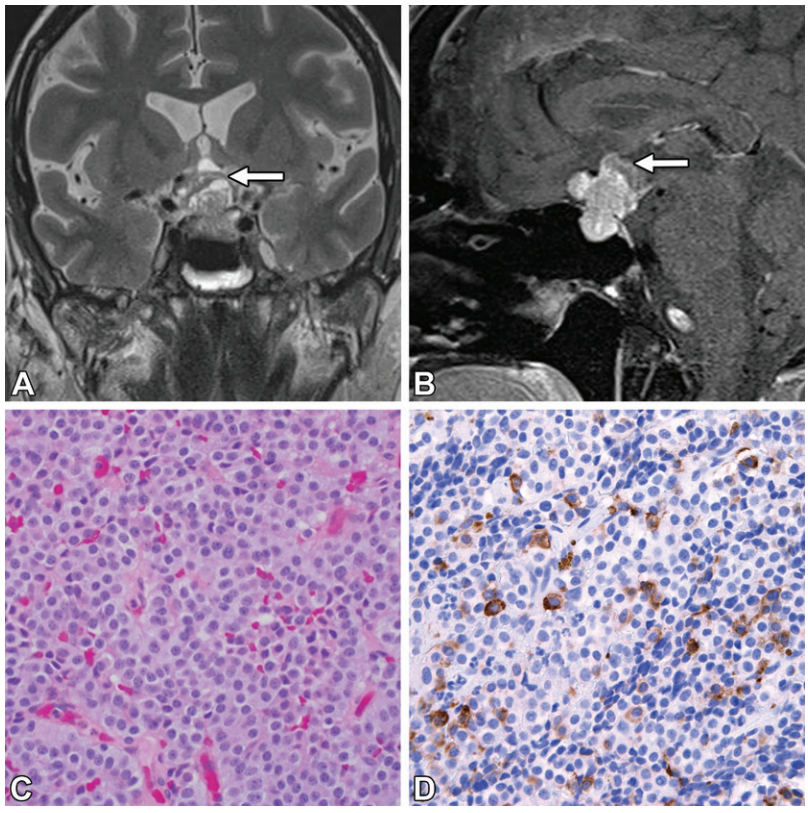

Figure 4. Silent corticotroph adenoma (corticotropinoma) in an older man with increasing headaches and peripheral vision loss. **(A)** Coronal T2-weighted MR image shows a heterogeneous lobulated intrasellar-suprasellar mass that expands the sella turcica and suprasellar cistern, effacing both the optic chiasm and anterior-inferior third ventricle superiorly (arrow). **(B)** Sagittal contrast-enhanced T1-weighted MR image shows solid enhancement of the suprasellar-intrasellar mass (arrow). Since there was no clinical or laboratory evidence of hormone hypersecretion (the patient underwent treatment for compressive hypopituitarism with a hydrocortisone replacement regimen), the statistically most likely diagnosis was a nonfunctioning or silent pituitary macroadenoma. **(C)** High-power hematoxylin-eosin (H-E) photomicrograph shows a monomorphic appearance of tumor cells in glandlike formations. The normal pituitary gland is less uniform owing to its variety of hormone-producing cells. Note the higher cellularity, with the closely packed round blue nuclei, which can contribute to higher attenuation at CT and lower signal intensity at T2-weighted MRI in many pituitary adenomas (as seen in Fig 2). **(D)** High-power photomicrograph with scattered positive (brown) immunostaining for ACTH indicates a corticotroph adenoma, specifically a silent corticotropinoma, because there was no hormone excess.

double adenoma (~1% incidence as well) represents two separate tumors of different cell lines arising within the same pituitary gland. Most plurihormonal adenomas manifest as macroadenomas, while most double adenomas manifest as microadenomas (18). Newly defined Pit-1 lineage adenoma (previously known as silent subtype 3 adenoma) is an example of a plurihormonal adenoma, which is usually silent, although some patients may have hyperprolactinemia, acromegaly, or hyperthyroidism. This neoplasm garners special interest because of its aggressive behavior, invasion of adjacent structures, high rate of recurrence, and low rate of disease-free survival (7,18).

Aggressive versus Invasive Adenoma

Pituitary adenomas that demonstrate rapid growth, early recurrence, or failure to respond to therapy are commonly termed *aggressive* (7,19). The term *invasive* is used for imaging, surgical, or histopathologic evidence of local extension into the cavernous sinus, sphenoid sinus, or clivus (4,7,19). Besides the plurihormonal Pit-1 lineage adenoma described previously, other potentially aggressive tumors with higher rates of recurrence include lactotroph adenoma in men, sparsely granulated somatotroph adenoma, silent corticotroph adenoma, and Crooke cell adenoma (4,7).

Collision Tumors

A number of other sellar or parasellar masses have been reported in association with pituitary adenomas, creating so-called collision tumors, (eg, Rathke cleft cyst [RCC], craniopharyngioma, pituicytoma, colloid cyst, arachnoid cyst, epidermoid cyst, hypophysitis, sarcoidosis, and some nonpituitary masses) (20). Gangliocytoma rarely arises in the sella (0.25%–1.3% of sellar tumors), usually in combination with a pituitary macroadenoma and manifesting calcification in 25% of cases (21).

Pituitary Carcinoma

Pituitary carcinoma is rare (<0.5% of all pituitary masses). Most are functional neoplasms, showing effects of hyperprolactinemia or hypercortisolemia (8,22). By definition, they are associated with cerebrospinal or systemic metastatic spread (7). Persistently elevated hormone levels after gross total resection of a presumed functional adenoma may prompt evaluation for metastatic disease. Most are believed to evolve from aggressive adenomas, although de novo development is also possible (22). There are no histopathologic features to distinguish pituitary carcinoma from adenoma (7,22). The imaging appearance is usually that of a macroadenoma but with additional intracranial or osseous lesions, similar to other

solid cancer metastases. The prognosis is poor, with 80% mortality (22).

Pituitary Blastoma

An infant with Cushing syndrome and a pituitary mass should prompt consideration of pituitary blastoma, a recently recognized rare primitive malignant neoplasm arising from the fetal anterior pituitary (23). It is most commonly seen in children less than 2 years of age (median age, 8 months) and is associated with DICER1 syndrome, an autosomal dominant condition with a unique constellation of hamartomatous, hyperplastic, or neoplastic lesions that involve the head, neck, thorax, and abdomen (7,23,24). Pituitary blastoma can be low or high grade and can vary in imaging appearance from a small solid pituitary mass to a large heterogeneous solid-cystic mass mimicking a macroadenoma. The location contributes to a poor prognosis and a 50% mortality rate (23,24).

Neuroimaging

MRI is the modality of choice for evaluation of the pituitary and parasellar region (25,26). A typical protocol includes pre- and postcontrast (before and after administration of contrast material, respectively) sagittal and coronal T1-weighted plus coronal T2-weighted spin-echo sequences performed with a 1.5-T or 3.0-T imaging unit using a reduced field of view focused on the sellar region (25). Pituitary adenomas typically show delayed enhancement and washout relative to that of a normal gland on postcontrast images (25,26). An additional dynamic postcontrast sequence can sometimes be helpful for accentuating differential enhancement and delineating tumor, such as in the setting of clinically suspected microadenoma (25).

The T2-weighted sequence is helpful in narrowing differential considerations and assessing effects of therapy. Prolactinomas in women tend to show mild T2 hyperintensity that becomes more pronounced after cabergoline therapy. Silent corticotropinomas show a characteristic microcystic pattern, which is not seen on pre- or postcontrast T1-weighted images (27). In the setting of acromegaly, somatotropinomas with low T2 signal intensity are more likely to represent a densely granulated tumor and to respond to somatostatin analogs (27,28). Cavernous sinus invasion by macroadenomas is best appreciated on T2-weighted images, particularly when using volumetric sequences (27,29). When evaluating a cystic sellar mass, T2-weighted imaging features such as fluid-fluid level, hypointense rim, septation, and off-midline location are more commonly associated with pituitary adenomas (30).

The increased signal intensity of 3-T MRI is beneficial in detection of very small microadenomas, for example in the setting of Cushing syndrome, particularly when combined with dynamic enhancement and spoiled gradient-echo sequences (14,31,32). Complementary postcontrast T2-weighted fluid-attenuated inversion-recovery (FLAIR) imaging has shown value, with delayed washout causing conspicuous focal hyperintensity of a microadenoma (33). Preoperative localization of a microadenoma is strongly associated with a successful surgical outcome and underscores the importance of accurate imaging (31).

Because of their larger size, macroadenomas are easier to identify at cross-sectional imaging. Aside from an expanded pituitary contour, displacement of the infundibulum and suprasellar extension are common, with optic chiasm and/or nerve compression, cavernous sinus invasion, and erosion of the sellar margin seen in larger tumors. The Hardy and Knosp classification systems have been used to quantitate the degree of invasion into the sella and parasellar regions by these macroadenomas.

The older Hardy system—based on radiographic findings—focused on distortion and destruction of the osseous sella margins, while the Knosp system assesses the impact of the tumor on the cavernous sinus laterally and encasement of the internal carotid artery (ICA), on the basis of MRI findings (34,35). The Knosp classification includes five grades: grade 0 (normal), grade 1 (extension to medial 50% of cavernous ICA), grade 2 (extension to lateral 50% of cavernous ICA), grade 3 (extension beyond lateral margin of cavernous ICA), and grade 4 (complete encasement of cavernous ICA) (35). A higher grade implies higher likelihood of cavernous sinus invasion, which translates into greater surgical risk and lower likelihood of gross total resection (25).

Head CT is usually the initial imaging modality of choice for acute-onset neurologic symptoms, including the characteristic visual loss (bitemporal hemianopsia) seen in pituitary apoplexy, and is able to quickly help confirm the presence of an intrasellar-suprasellar mass compressing the optic chiasm. While CT hyperattenuation may be evident in the first few hours, MRI is superior for demonstrating initial T1 isointensity and T2 hypointensity, followed by subsequent T1 and T2 hyperintensity, often with a fluid-fluid level, reflecting evolution of intratumoral blood products (Fig 5). Surgery remains the primary method of treatment, although an increasing number may be managed conservatively (12).

Advanced imaging techniques have been used to assess tumor consistency and help predict re-

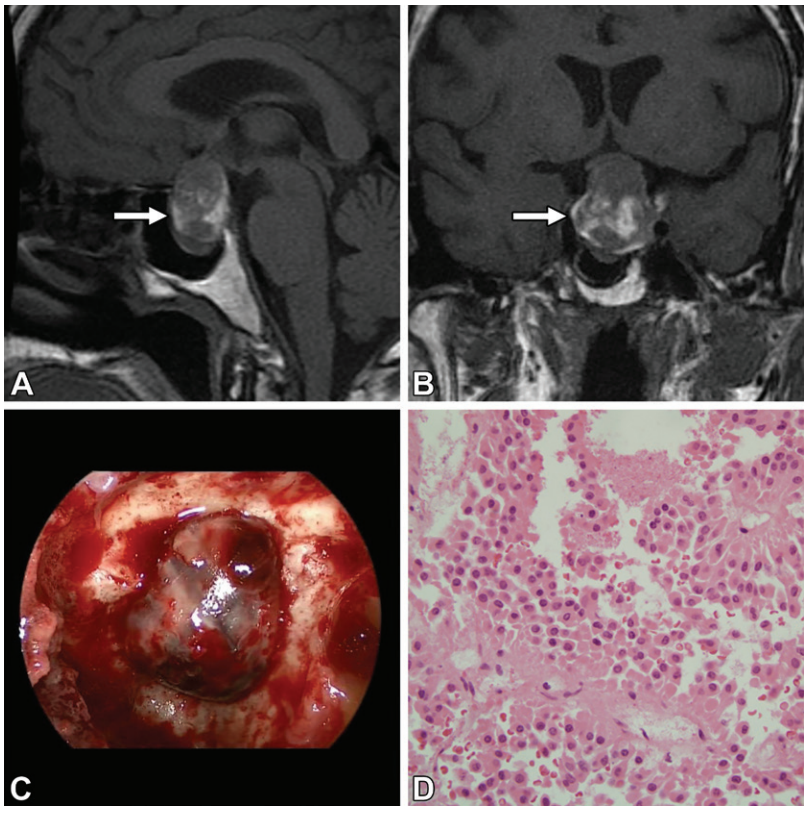

Figure 5. Pituitary apoplexy due to a null cell macroadenoma in an older man with sudden-onset headache and visual loss in the left eye (with a temporal field deficit on the right). **(A)** Sagittal T1-weighted MR image shows a large expansile intrasellar-suprasellar mass and patchy internal hyperintensity (arrow), consistent with intratumoral hemorrhage. **(B)** Coronal T1-weighted MR image shows a large expansile intrasellar-suprasellar mass with intrinsic T1 hyperintensity (arrow) and compression of the optic chiasm superiorly. The acute presentation is from hemorrhagic infarct with sudden enlargement of a preexisting macroadenoma. There was no tumoral enhancement on contrast-enhanced images (not shown) owing to the extensive intratumoral hemorrhage. **(C)** Intraoperative endoscopic photograph during emergency transsphenoidal surgical decompression after exposure of the sellar floor shows a purplish mass consistent with hemorrhagic macroadenoma. **(D)** High-power H-E photomicrograph shows monomorphic adenoma cells (similar to those seen in Fig 4), now accompanied by large areas of pink acellular necrosis and scattered red blood cells. Tumor cells were negative for hormones at immunohistochemical analysis (not shown), suggestive of a rare null cell adenoma.

sponse to therapy. Relative noncontrast T1 signal intensity, MR elastography, and textural analysis have shown utility in assessment of the firmness of macroadenomas before surgical resection (36–38). Radiomic modeling has been shown to improve preoperative prediction of treatment response in patients with an invasive functional pituitary macroadenoma (39).

By definition, rare ectopic pituitary adenomas occur exclusively outside the sella turcica and are believed to arise from embryologic pituitary remnants along the migrational path of Rathke pouch from the nasopharynx through the sphenoid body and/or sinus (Fig 6) (40,41). Erosion or destruction of the sinus wall is frequently noted for those arising within the sphenoid sinus (40). Involvement of the nasal cavity, ethmoid sinus, temporal bone, nasal bridge, suprasellar cistern, Meckel cave, cavernous sinus, and thalamus is less common (32,40).

Other imaging modalities have more limited utility in evaluation of pituitary adenomas. CT excels in helping identify osseous effects in the sella and adjacent skull base for larger tumors. Dynamic contrast-enhanced CT may be performed for microadenomas when MRI is contraindicated (42). Pituitary adenomas may demonstrate radiotracer uptake at PET, including carbon 11 methionine for recurrent or ACTH-secreting adenomas (25).

Common things being common, a pituitary adenoma belongs in the differential diagnosis for any solid or mixed solid-cystic mass arising from the adenohypophysis in adults or older children (consider a pituitary blastoma in younger children). Involvement of the anterior pituitary lobe and

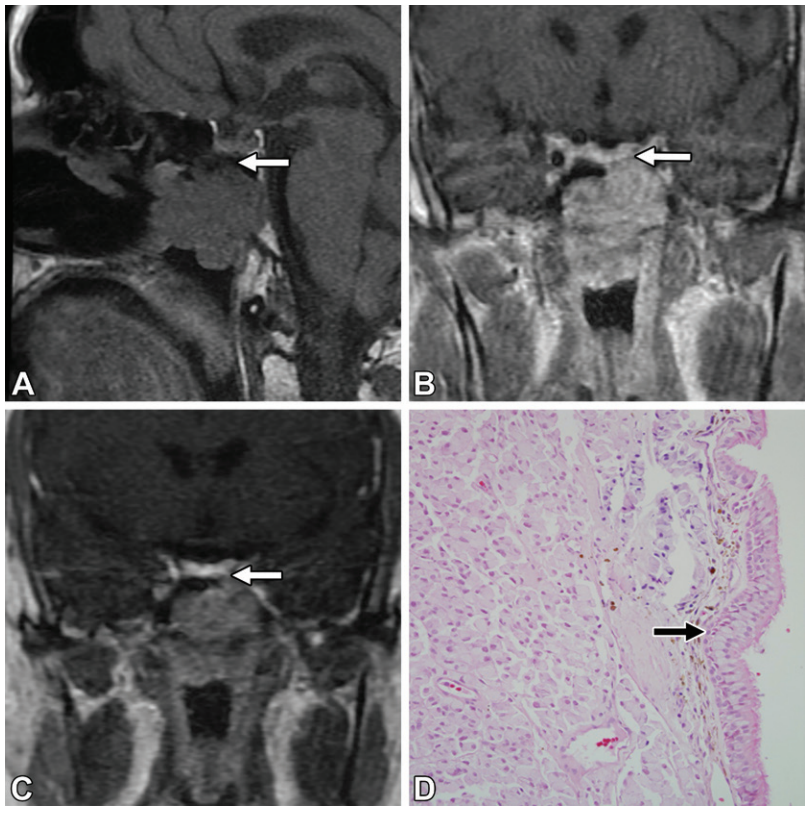

Figure 6. Ectopic corticotroph adenoma (corticotropinoma) in a middle-aged man with symptomatic hypercortisolemia (Cushing syndrome) and elevated serum ACTH levels. **(A)** Sagittal T1-weighted MR image shows a lobulated mass, centered around the junction of the nasopharynx and sphenoid body, clearly separate (arrow) from the normal pituitary gland superiorly. **(B)** Coronal contrast-enhanced T1-weighted MR image shows homogeneous enhancement of the lobulated nasopharyngeal-sphenoid mass, clearly separate (arrow) from the enhancing pituitary gland superiorly. In this location, the differential diagnosis includes carcinoma arising from the nasopharynx or sphenoid sinus, extranodal non-Hodgkin lymphoma, and a rare ectopic ACTH-secreting pituitary macroadenoma. **(C)** Coronal dynamic contrast-enhanced T1-weighted MR image shows a delayed enhancement pattern of the ectopic ACTH-secreting macroadenoma when compared with the normal pituitary gland superiorly (arrow), similar to what one would expect with a much more common orthotopic pituitary adenoma. **(D)** Low-power H-E photomicrograph shows a monomorphic population of neuroendocrine tumor cells on the left side, adjacent to a vertical strip of respiratory-type pseudostratified columnar epithelium on the right side (arrow), representing normal sphenoid sinus mucosa. Immunostaining for ACTH expression was extensively positive (not shown) and confirmed a diagnosis of Cushing disease by ectopic adenoma, which is rare but can arise anywhere along the embryonic path of Rathke pouch.

expansion of the bony sella turcica are useful clues. Metastasis or lymphoma of the adenohypophysis is also possible but relatively rare. Symmetrical enlargement of the adenohypophysis should prompt consideration of nonneoplastic causes such as pituitary hyperplasia, lymphocytic hypophysitis, or drug-related hypophysitis in the clinical settings of end-organ failure (eg, hypothyroidism), peripartum endocrine deficiencies, or T-cell activating immunotherapy (eg, for melanoma). A decision to perform biopsy versus observation depends on the clinical setting, including the presence or absence of visual or hormonal abnormalities.

Primary Tumors of Rathke Pouch (Embryonic Precursor)

The second section reviews the clinical, pathologic, and radiologic features of two sellar region masses (one nonneoplastic cyst plus one neoplastic entity) that arise from the embryonic precursor of the adenohypophysis (Rathke pouch or craniopharyngeal duct). Their neuroimaging and histopathologic characteristics reflect their origin from oral ectoderm, which has not yet differentiated into the mature neuroendocrine cells of the anterior pituitary gland. The nonneoplastic cyst is discussed because it is common and reinforces embryology-based pathophysiology.

Rathke Cleft Cyst

Martin Heinrich Rathke, one of the founders of modern embryology, developed the theory of development of the adenohypophysis from an outpouching of the oral stomodeum (Rathke pouch), forming the pars distalis, pars tuberalis, and pars intermedia of the anterior pituitary gland. If the pouch does not completely obliterate, a cystic remnant may persist in the cleft between the pars distalis and pars intermedia or in the pars tuberalis, producing a nonneoplastic RCC in the sellar or suprasellar region at the anterior margin of the neurohypophysis or infundibulum (43).

In a series of 1000 autopsy pituitary specimens, RCC was incidentally found in 11.3%, spanning all age ranges (least likely in the 0–29 years age group), usually measuring less than 2 mm (44). Mahdi et al (45) noted an incidental cyst or cystlike structure in nearly 60% of 232 pediatric pituitary glands on MR images, with a small average volume of less than 19 mm^3. Larger RCCs (>10 mm) are more likely to be symptomatic and may result in headache, visual impairment, or endocrine dysfunction (46). While patients most commonly present with symptoms in their mid-30s, symptoms may develop at any age and can be treated with cyst drainage (47).

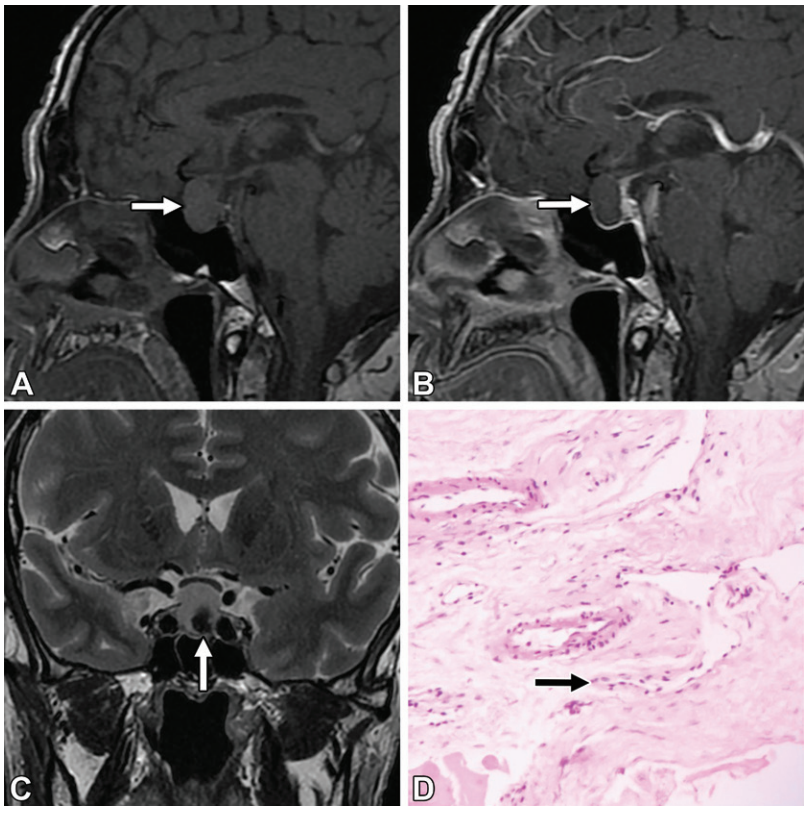

Figure 7. Rathke cleft cyst (symptomatic) in an older man with episodic headache. **(A)** Sagittal T1-weighted MR image shows an ovoid intrasellar-suprasellar lesion with mild intrinsic T1 hyperintensity (arrow), consistent with proteinaceous contents. **(B)** Sagittal contrast-enhanced T1-weighted MR image shows no solid or nodular enhancement in the lesion (arrow), which is suggestive of a nonneoplastic cyst rather than a vascularized neoplasm. An initial differential diagnosis for a cystic mass in the sellar region will include pituitary adenoma with cystic or hemorrhagic degeneration, craniopharyngioma (especially adamantinomatous), and RCC (favored here). **(C)** Coronal T2-weighted MR image shows mild indentation of the optic chiasm superiorly and a small T2-hypointense intracystic nodule (arrow), characteristic of RCC but not seen in all cases. **(D)** Low-power H-E photomicrograph shows a nonspecific collapsed epithelial lining (arrow), consistent with a cyst. There was no evidence of pituitary adenoma, craniopharyngioma, or any other neoplasm.

Histopathologically, RCCs are epithelium-lined cysts, usually characterized by a respiratory-type ciliated columnar or cuboidal epithelium with goblet cells (48). Significant squamous metaplasia of the cyst wall has been associated with increased risk of recurrence (49). Intracystic nodules may be seen and are composed of mucin, protein, and cholesterol components (50). RCC lacks the genetic markers that are often seen in adamantinomatous craniopharyngioma (*CTNNB1* mutation) (51) and in papillary craniopharyngioma (*BRAF* V600E mutation) (52).

Radiologically, larger symptomatic RCCs are typically intrasellar-suprasellar in location (Fig 7). Smaller RCCs may be purely intrasellar, with a rare location being purely suprasellar (48,53,54). The cyst can have variable T1 and T2 signal intensities, with a majority having T1 iso- or hyperintense signal and T2 hyper- or hypointense signal (54). An intracystic nodule may be found in up to 77% of lesions (50,54,55), typically exhibiting T1 hyperintense and T2 hypointense signal relative to that of white matter (50), although variable low T1 signal intensity has been described (54).

Solid or nodular enhancement does not occur in RCC, although thin peripheral enhancement may result from compression of normal adjacent pituitary tissue or inflammation of the wall (50,53). Contrast-enhanced three-dimensional T2-weighted FLAIR imaging has shown a significant difference in mural enhancement between RCC and cystic craniopharyngioma (56). Single-shot fast spin-echo diffusion-weighted imaging has demonstrated higher apparent diffusion coefficients in RCCs than in other cystic masses like craniopharyngiomas and hemorrhagic adenomas (57). In a retrospective review of pathologically confirmed RCCs, they were likely to be ovoid, small in volume (<2 mL), and purely cystic with no or thin (<2 mm) wall enhancement (58).

Craniopharyngioma

Craniopharyngioma is uncommon, with an incidence of 0.13 per 100 000 person-years, and the age distribution will vary depending on the subtype. Adamantinomatous craniopharyngiomas (ACPs) account for 90% of craniopharyngiomas, while (squamous) papillary craniopharyngiomas (PCPs) represent the remaining 10%. While PCP is nearly always found in adults, ACP has a bimodal distribution, peaking in children younger than 18 years of age and adults 40–60 years of age (59–61). Austrian pathologist Jakob Erdheim subtyped his "hypophyseal duct tumors" (*hypophyseal duct* meaning craniopharyngeal duct or Rathke pouch), which are now better known as craniopharyngiomas (62).

There are two leading theories of tumor pathogenesis: embryogenetic and metaplastic. The embryogenetic theory postulates that ACPs arise from epithelial remnants of Rathke pouch, which

is itself derived from the stomodeum (primitive mouth), which helps explain the odontogenic features at histopathologic analysis. It also helps explain why ACPs can arise anywhere along the embryologic path of Rathke pouch, from the craniopharyngeal canal within the sphenoid body to the intrasellar pars distalis and suprasellar pars tuberalis. In contrast, the metaplastic theory postulates that PCPs are derived from the portion of the stomodeum that becomes buccal mucosa and therefore undergoes metaplastic change to squamous epithelium in the region of the pars tuberalis (63,64).

Children may present with headache, vomiting, visual loss, lethargy, polydipsia and/or polyuria, and rarely cognitive and/or behavioral disturbances and be diagnosed with endocrine dysfunction. The most common presenting signs involve visual loss and less commonly ataxia or reduction in level of consciousness (65,66). Weight gain tends to occur later in the disease process. Adults present with similar symptoms and signs as children but more often with cognitive impairment (67). Treatment of craniopharyngioma may consist of gross total or subtotal resection, plus or minus radiation therapy. Postoperative quality of life needs to be weighed in light of the significant consequences of treatment-related hypothalamic damage (65–68). Cystic decompression and instillation of sclerosing agents is a possible alternative (65,66).

Adamantinomatous versus Papillary

At gross examination, ACP tends to be lobulated and adherent to adjacent structures. Cystic components are seen in over 90% of ACPs and often contain so-called crankcase (machine) oil–type fluid with cholesterol crystals. Whereas calcifications are seen in most pediatric cases, roughly 40% of adult cases have calcification. Tumor margins can be infiltrative or irregular and may be accompanied by chronic inflammation or gliosis of adjacent brain. At histologic examination, there is central stellate reticulum and peripheral palisading epithelium with associated nodules of anucleate "ghost cells" (wet keratin), which are considered pathognomonic. Genetically, most ACPs harbor a mutation in the β-catenin gene *(CTNNB1)*, resulting in both nuclear and cytoplasmic accumulation of β-catenin (Fig 8), while PCPs demonstrate only normal accumulation in the cytoplasmic membrane (69). Owing to the embryologic relationship with the stomodeum, ACPs can express odontogenic markers (eg, enamelin) and share histopathologic similarities (*CTNNB1* mutation) with calcifying odontogenic cysts (60,61).

In contrast, PCP tends to be a more discrete, encapsulated, spherical, and solid mass with an occasional unilocular cystic component. Calcifications are rare. Histologically, PCP is composed of well-differentiated nonkeratinizing squamous epithelium and pseudopapillae with fibrovascular cores. PCP lacks the stellate reticulum, ghost cells, and odontogenic features of ACP. PCP may demonstrate goblet cell formation and foci of ciliation, reminiscent of RCC (60,61). PCP lacks the *CTNNB1* mutation and will not show strong nuclear and cytoplasmic accumulation of β-catenin. However, PCP is associated with a *BRAF* gene mutation (V600E) throughout the squamous-papillary epithelium, which is not seen in ACP and which can be identified with VE1 antibody immunohistochemicial analysis (69). Presence or absence of this mutation can also help differentiate between PCP and RCC with extensive squamous metaplasia, as PCP will harbor the mutation whereas RCC will not (70).

Neuroimaging

At CT and MRI, ACPs are usually cystic or predominantly cystic and located above the sella (Fig 9), although roughly one-fourth will be both intrasellar and suprasellar. ACP is more commonly lobulated, versus the more rounded shape for PCP. Cystic components can show variable signal intensity with T1-weighted and T2-weighted sequences, depending on protein content, and solid components show avid enhancement (63). At CT, ACP will often show associated calcification, especially in pediatric patients. When differentiating from PCP, tumoral calcification and intrinsic T1 hyperintensity (protein content) are significantly associated with the adamantinomatous subtype (Fig 10) (71).

On CT and MR images, PCPs are more often solid or mixed solid-cystic lesions, commonly arising above the sella, with only occasional pure intrasellar location. Unlike ACP, PCP tends to be more spherical in shape. Solid components show avid enhancement, which is often heterogeneous and associated with high T2 signal intensity. Occasional cystic components will be T1 hypointense and T2 hyperintense because the contents are less proteinaceous than in ACP (Fig 11). Unlike ACP, it is relatively rare for PCP to demonstrate calcification at CT or to encase subarachnoid vessels in the suprasellar cistern (63).

Primary Tumors of Neurohypophysis

The most recent 2016 World Health Organization classification of CNS tumors lists four entities under "tumours of the sellar region" (remember that pituitary adenomas are categorized as endocrine not CNS tumors): craniopharyngioma, pituicytoma, granular cell tumor (GCT), and spindle cell oncocytoma (SCO) (72). While SCO

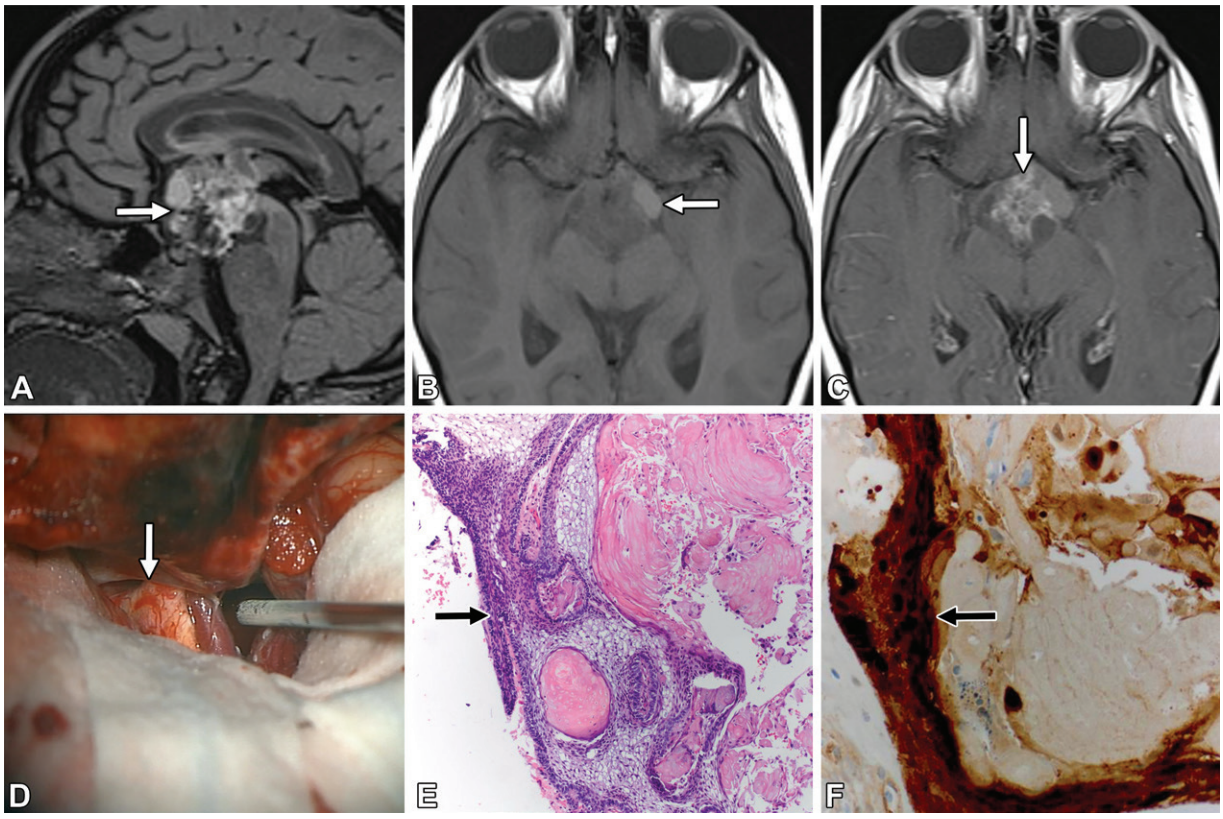

Figure 8. Adamantinomatous craniopharyngioma in a child with growth deceleration from pediatric hypopituitarism. **(A)** Sagittal T2-weighted FLAIR MR image shows a large markedly heterogeneous mass (arrow) centered in the suprasellar cistern, which effaces the anterior third ventricle and hypothalamus superiorly (normal pituitary gland can be seen inferiorly). **(B)** Axial T1-weighted MR image shows a mostly isointense mass filling the suprasellar cistern and a small ovoid pocket of intrinsic hyperintensity on the left side, representing proteinaceous fluid (arrow). **(C)** Axial contrast-enhanced T1-weighted MR image shows a mixed solid-cystic tumor with enhancing solid components centrally (arrow) and nonenhancing cystic components peripherally, including the higher-T1-signal-intensity cyst with proteinaceous fluid on the left side (ie, crankcase or machine oil contents). **(D)** Intraoperative photograph from the lateral pterional transsylvian approach for microsurgical resection of the suprasellar mass shows a reddish internal carotid artery in the center of the image, plus the whitish tumor with surface vascularity on the left side (arrow). Given a normal pituitary gland, a transsphenoidal approach would have been ineffective in this case and is indicated for sellar masses (as seen in Fig 5). **(E)** Low-power H-E photomicrograph shows typical histologic features of adamantinomatous (resembling enamel organ) craniopharyngioma. On the left side, purple basaloid epithelial cells (arrow) surround the white looser stellate reticulum. On the right side, pink pearls of anucleate ghost cells slough off into a cystic cavity. This finding is also known as wet keratin and is considered a characteristic feature. The histopathology is much more heterogeneous than in an adenoma and is reflected in the neuroimaging findings. **(F)** Low-power photomicrograph with β-catenin immunostain (brown areas) shows strong nuclear and cytoplasmic expression (arrow), indicating ACP (*CTNNB1* mutation).

was initially thought to arise from nonendocrine folliculostellate cells within the anterior pituitary gland, these three entities are now all thought to arise from specialized glial cells (pituicytes) within the posterior pituitary gland: "pituicytomas, granular cell tumors of the sellar region and spindle cell oncocytomas show nuclear expression of thyroid transcription factor 1 (TTF-1), suggesting that these three tumors may constitute a spectrum of a single neurological entity" (7). Along this spectrum, some distinguishing ultrastructural features at electron microscopy would include abundance of cytoplasmic granules in GCT and cytoplasmic mitochondria in SCO, which is similar to other GCTs and oncocytomas outside of the sellar region (73).

At the macroscopic or neuroimaging level, it can be difficult or impossible to distinguish these pituicyte-derived neoplasms from each other or from the much more commonly encountered pituitary adenoma, without the benefit of microscopic analysis. All of these entities, including silent or nonsecretory macroadenomas, can manifest radiologically with solid enhancing intrasellar or suprasellar masses and clinically with headache, visual disturbance, hyperprolactinemia from infundibular compression (stalk effect), hypopituitarism from adenohypophyseal compression, and rarely diabetes insipidus (73). If the solid enhancing mass is small enough to be clearly identified as arising from the neurohypophysis or infundibulum, not the adenohypophysis, then pituicytoma belongs in the differential diagnosis in either location (Fig 12), to be supplemented by GCT if the mass is suprasellar arising from the infundibulum (74). Because SCO is often

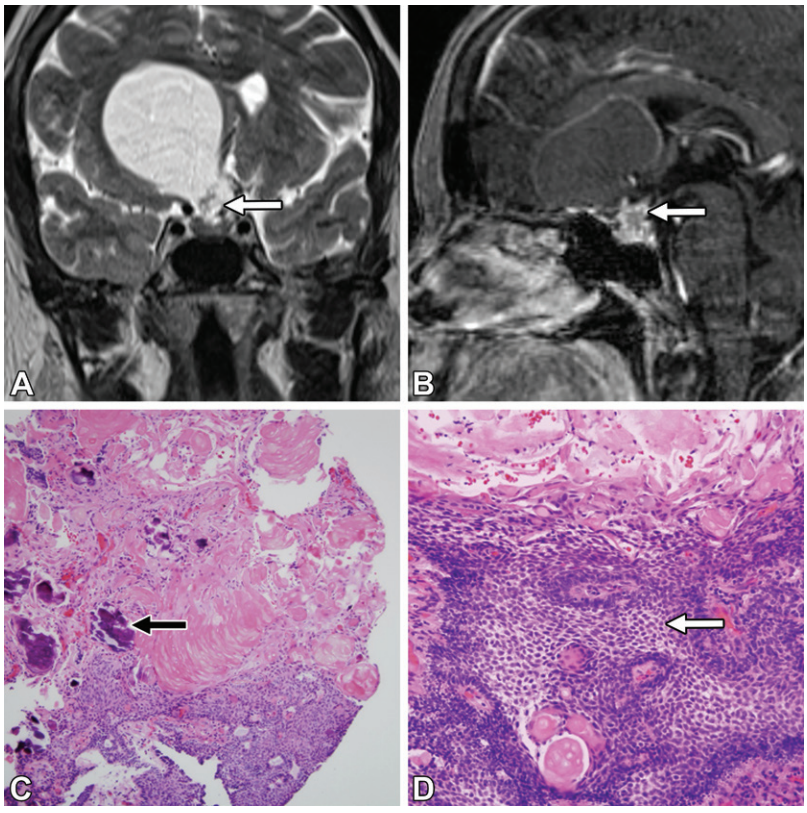

Figure 9. Adamantinomatous craniopharyngioma in an older woman with syncope. **(A)** Coronal T2-weighted MR image reveals a large cystic mass in the sellar region that extends into the right frontal lobe. There is mild complexity and nodularity at the inferior and suprasellar portion of the cyst (arrow), which is located above a normal-appearing pituitary gland. **(B)** Sagittal contrast-enhanced T1-weighted MR image shows a mixed cystic-solid mass. There is a larger nonenhancing cystic component at the inferior frontal lobe, with a smaller enhancing solid or nodular component (arrow), located above a normal-appearing pituitary gland. As a rule, a suprasellar mass with prominent cysts or calcifications will prompt consideration of ACP. **(C)** Low-power H-E photomicrograph shows characteristic histologic findings of ACP, including blue basaloid squamous epithelium at the bottom, pink nodules of wet keratin desquamation at the top, and purple foci of intratumoral calcifications on the left side (arrow). **(D)** High-power H-E photomicrograph of the blue squamous epithelium shows peripheral palisading of darker basaloid cells around lighter, looser, plumper cells in the center, which is also known as stellate reticulum (arrow). Note the pink pearl of wet keratin at the bottom of the image, left of center.

characterized by aggressive infiltrative growth and usually manifests as a large intrasellar-suprasellar mass, it is easily mistaken for a nonfunctional adenohypophyseal macroadenoma at preoperative neuroimaging—an unexpected "zebra" amid a sea of "horses" (75).

Conclusion

In summary, primary tumors of the pituitary gland can be subcategorized as common primary tumors of the adenohypophysis (eg, pituitary adenoma), uncommon primary tumors of Rathke pouch (ie, craniopharyngioma), and rare primary tumors of the neurohypophysis (eg, pituicytoma). Most of these neoplasms manifest as enhancing masses in the sellar and/or suprasellar region, sometimes with prominent cystic components. Most of the time, the diagnosis will be a pituitary adenoma and either medical or surgical therapy may be offered, depending on the functional status and size of the tumor. The neuroimaging appearance of cystic macroadenomas can overlap with that of RCC or ACP. Pituicyte-derived neoplasms are rare considerations for solid enhancing masses arising from the neurohypophysis or infundibulum. In the end, a definitive diagnosis depends on histopathologic analysis results, often supplemented by immunohistochemical stains for specific pituitary hormones or transcription factors.

***Disclosures of Conflicts of Interest.*—K.K.K.** *Activities related to the present article:* consulting agreement with Mayo Clinic to provide support, as the Section Chief of Neuroradiology, for the American Institute for Radiologic Pathology, a program of the American College of Radiology. *Activities not related to the present article:* consulting agreement with Mayo Clinic to provide support, as the Section Chief of Neuroradiology, for the

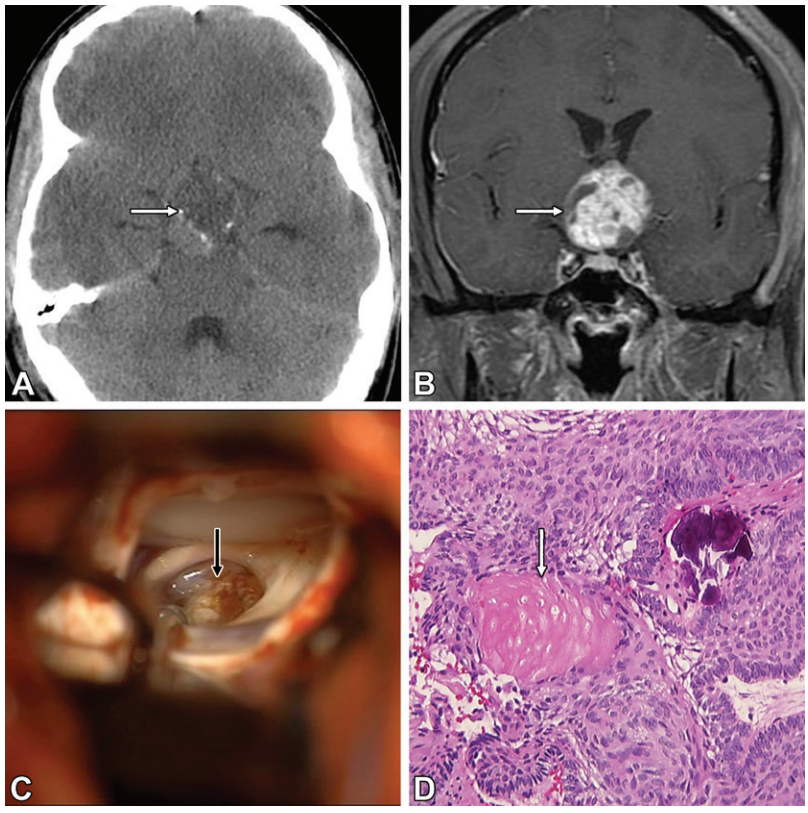

Figure 10. Adamantinomatous craniopharyngioma in a young man with headaches and blurry vision. **(A)** Axial head CT image shows a heterogeneous and partially cystic mass centered in the suprasellar cistern, along with tiny peripheral calcifications (arrow). **(B)** Coronal contrast-enhanced T1-weighted image from subsequent brain MRI shows a round mixed solid-cystic suprasellar mass (arrow) located above the normal pituitary gland. These imaging findings, specifically the calcifications and location, favor an uncommon diagnosis of ACP over the much more common diagnosis of pituitary adenoma in the sellar region. **(C)** Intraoperative photograph from a superior interhemispheric transcallosal approach for microsurgical resection of the suprasellar mass shows a whitish tumor with surface vascularity in the window (arrow). A transsphenoidal approach would have been ineffective for this suprasellar mass (similar to that in Fig 8). **(D)** High-power H-E photomicrograph shows a close-up view of a pink pearl of wet keratin on the left (arrow) and a purple focus of tumoral calcification on the right, both in a background of blue palisading squamous epithelium. The histologic findings are diagnostic of ACP.

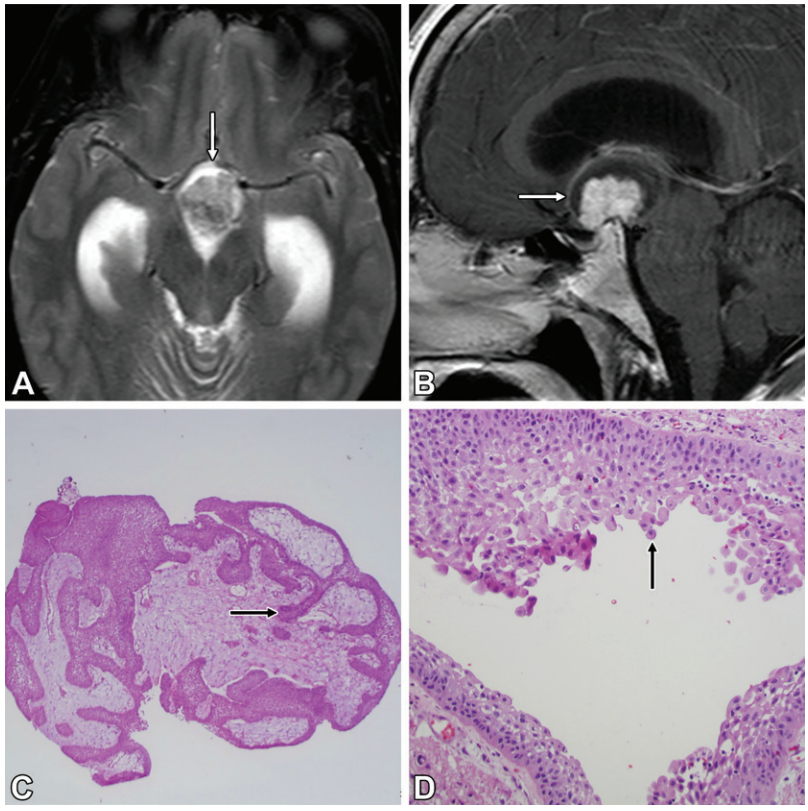

Figure 11. Papillary craniopharyngioma in a young adult man with worsening headache. **(A)** Axial T2-weighted MR image shows a suprasellar mass, which is mostly solid with a small peripheral cystic component (arrow) and which is causing obstructive hydrocephalus with temporal horn dilatation. The patient was admitted for ventriculostomy and biopsy. **(B)** Sagittal contrast-enhanced T1-weighted MR image shows a mixed solid-cystic suprasellar mass, which has a central enhancing solid component plus a peripheral nonenhancing cystic component and effaces the third ventricle (arrow). A separate pituitary gland is depicted inferiorly and is compressed by the intracranial hypertension. These findings are suspicious for a craniopharyngioma, and in the absence of calcification or proteinaceous fluid, the uncommon papillary subtype would be a possibility for an adult. **(C)** Low-power H-E photomicrograph depicts a rounded mass with well-defined margins, where darker squamous epithelium forms crude pseudopapillae (arrow) around lighter fibrovascular cores. PCP has a blander architecture when compared with the adamantinomatous subtype (as seen in Figs 8–10). **(D)** High-power H-E photomicrograph of the well-differentiated nonkeratinizing squamous epithelium shows formation of pseudopapillae due to epithelial dehiscence (arrow). Note the absence of wet keratin, calcification, or other findings associated with the more common adamantinomatous subtype.

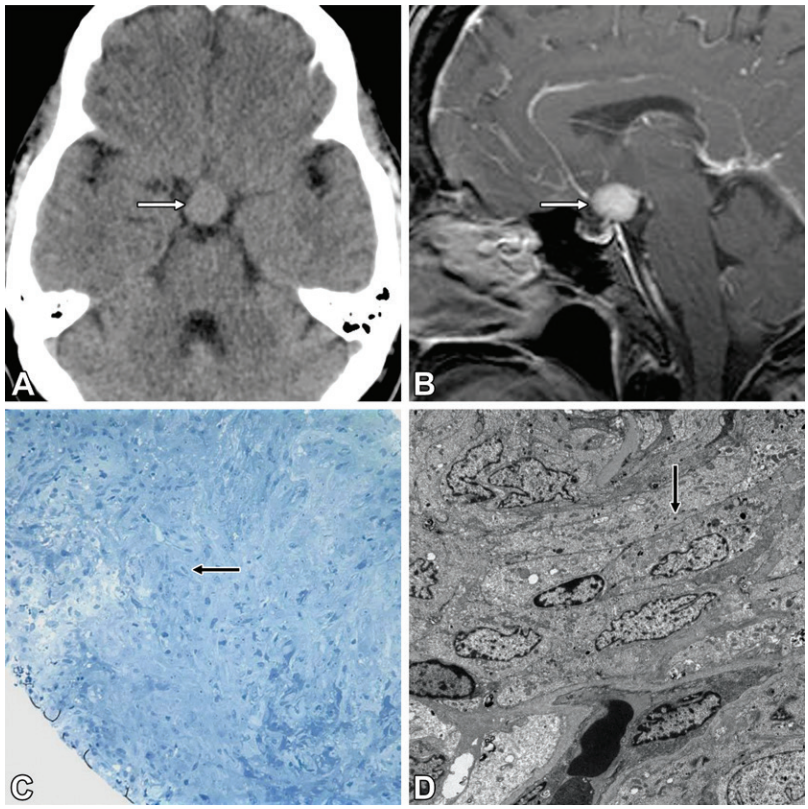

Figure 12. Pituicytoma in an older man who fell. **(A)** Axial head CT image shows an incidental finding of a round homogeneous mass centered in the suprasellar cistern (arrow). The mass is isoattenuating when compared with gray matter. **(B)** Sagittal contrast-enhanced T1-weighted MR image from a subsequent brain MRI examination shows a solid rounded homogeneously enhancing mass (arrow) that is centered on and appears to be arising from the pituitary stalk (infundibulum). While nonspecific, this finding should prompt inclusion of a rare neurohypophyseal tumor in the differential diagnosis, for example, a pituicytoma or GCT of the sellar region. Other considerations include an ectopic pituitary adenoma (along the embryonic path of Rathke pouch), lymphoma or neurosarcoidosis in adults, and germinoma or Langerhans cell histiocytosis in children. **(C)** Low-power toluidine blue photomicrograph shows a bland spindle cell neoplasm with oval to elongate nuclei (arrow) arranged in a fascicular pattern. There is no evidence of mitosis or necrosis. The histologic appearance differs from the monomorphic neuroendocrine cells with rounded nuclei seen in pituitary adenoma (as seen in Figs 3–6) or the squamous epithelium seen in craniopharyngioma (as seen in Figs 8–11). **(D)** Electron microscopic image shows multiple spindle-shaped elongate nuclei and small scattered cytoplastic neuroendocrine-type granules (arrow), but not in sufficient quantity to make a diagnosis of GCT. Immunohistochemical analysis results can also support a diagnosis of pituicytoma (eg, immunostain for TTF-1).

American Institute for Radiologic Pathology, a program of the American College of Radiology. *Other activities:* disclosed no relevant relationships.

References

1. Ostrom QT, Cioffi G, Gittleman H, et al. CBTRUS Statistical Report: Primary Brain and Other Central Nervous System Tumors Diagnosed in the United States in 2012-2016. Neuro Oncol 2019;21(suppl 5):v1–v100.
2. Ostrom QT, Gittleman H, de Blank PM, et al. American Brain Tumor Association Adolescent and Young Adult Primary Brain and Central Nervous System Tumors Diagnosed in the United States in 2008-2012. Neuro Oncol 2016;18(suppl 1):i1–i50.
3. Amar AP, Weiss MH. Pituitary anatomy and physiology. Neurosurg Clin N Am 2003;14(1):11–23, v.
4. Di Ieva A, Rotondo F, Syro LV, Cusimano MD, Kovacs K. Aggressive pituitary adenomas: diagnosis and emerging treatments. Nat Rev Endocrinol 2014;10(7):423–435.
5. Molitch ME. Diagnosis and Treatment of Pituitary Adenomas: A Review. JAMA 2017;317(5):516–524.
6. Marques P, Korbonits M. Genetic Aspects of Pituitary Adenomas. Endocrinol Metab Clin North Am 2017;46(2):335–374.
7. Lopes MBS. The 2017 World Health Organization classification of tumors of the pituitary gland: a summary. Acta Neuropathol (Berl) 2017;134(4):521–535.
8. Nose V, Grossman A, Mete O. Lactotroph adenoma. In: Lloyd RV, Osamura RY, Kloppel G, Rosai J, eds. WHO Classification of Tumours of the Endocrine Organs. 4th ed. Lyon, France: IARC Press, 2017; 24–27.
9. Lemelin A, Lapoirie M, Abeillon J, et al. Pheochromocytoma, paragangliomas, and pituitary adenoma: an unusual association in a patient with an SDHD mutation—case report. Medicine (Baltimore) 2019;98(30):e16594.
10. Mete O, Asa SL. Clinicopathological correlations in pituitary adenomas. Brain Pathol 2012;22(4):443–453.
11. Osamura RY, Grossman A, Korbonits M, et al. Pituitary adenomas. In: Lloyd RV, Osamura RY, Kloppel G, Rosai J, eds. WHO Classification of Tumours of the Endocrine Organs. 4th ed. Lyon, France: IARC Press, 2017; 14–18.
12. Singh TD, Valizadeh N, Meyer FB, Atkinson JLD, Erickson D, Rabinstein AA. Management and outcomes of pituitary apoplexy. J Neurosurg 2015;122(6):1450–1457.
13. Mete O, Korbonits M, Osamura RY, Trouillas J, Yamada S. Somatotroph adenoma. In: Lloyd RV, Osamura RY, Kloppel G, Rosai J, eds. WHO Classification of Tumours of the Endocrine Organs. 4th ed. Lyon, France: IARC Press, 2017; 19–23.
14. Mete O, Grossman A, Trouillas J, Yamada S. Corticotroph adenoma. In: Osamura RY, Lloyd RV, Kloppel G, Rosai J, eds. WHO Classification of Tumours of the Endocrine Organs. 4th ed. Lyon, France: IARC Press, 2017; 30–33.
15. Erickson D, Erickson B, Watson R, et al. 3 Tesla magnetic resonance imaging with and without corticotropin releasing hormone stimulation for the detection of microadenomas in Cushing's syndrome. Clin Endocrinol (Oxf) 2010;72(6):793–799.
16. Osamura RY, Grossman A, Nishioka H, Trouillas J. Thyrotroph adenoma. In: Lloyd RV, Osamura RY, Kloppel G, Rosai J, eds. WHO Classification of Tumours of the Endocrine Organs. 4th ed. Lyon, France: IARC Press, 2017; 28–29.
17. Nishioka H, Kontogeorgos G, Lloyd RV, Lopes MBS, Mete O, Nose V. Null cell adenoma. In: Lloyd RV, Osamura RY, Kloppel G, Rosai J, eds. WHO Classification of Tumours of the Endocrine Organs. 4th ed. Lyon, France: IARC Press, 2017; 37–38.
18. Kontogeorgos G, Kovacs K, Lloyd RV, Righi A. Plurihormonal and double adenomas. In: Lloyd RV, Osamura RY, Kloppel G, Rosai J, eds. WHO Classification of Tumours of the Endocrine Organs. 4th ed. Lyon, France: IARC Press, 2017; 39–40.

19. Chatzellis E, Alexandraki KI, Androulakis II, Kaltsas G. Aggressive pituitary tumors. Neuroendocrinology 2015;101(2):87–104.
20. Koutourousiou M, Kontogeorgos G, Wesseling P, Grotenhuis AJ, Seretis A. Collision sellar lesions: experience with eight cases and review of the literature. Pituitary 2010;13(1):8–17.
21. Yang B, Yang C, Sun Y, et al. Mixed gangliocytoma-pituitary adenoma in the sellar region: a large-scale single-center experience. Acta Neurochir (Wien) 2018;160(10):1989–1999.
22. Roncaroli F, Kovacs K, Lloyd RV, Matsuno A, Righi A. Pituitary carcinoma. In: Lloyd RV, Osamura RY, Kloppel G, Rosai J, eds. WHO Classification of Tumours of the Endocrine Organs. 4th ed. Lyon, France: IARC Press, 2017; 41–44.
23. Rotondo F, Syro LV, Lloyd RV, Foulkes WD, Kovacs K. Pituitary blastoma. In: Lloyd RV, Osamura RY, Kloppel G, Rosai J, eds. WHO Classification of Tumours of the Endocrine Organs. 4th ed. Lyon, France: IARC Press, 2017; 45.
24. Guillerman RP, Foulkes WD, Priest JR. Imaging of DICER1 syndrome. Pediatr Radiol 2019;49(11):1488–1505.
25. Bashari WA, Senanayake R, Fernández-Pombo A, et al. Modern imaging of pituitary adenomas. Best Pract Res Clin Endocrinol Metab 2019;33(2):101278.
26. Newton DR, Dillon WP, Norman D, Newton TH, Wilson CB. Gd-DTPA-enhanced MR imaging of pituitary adenomas. AJNR Am J Neuroradiol 1989;10(5):949–954.
27. Bonneville JF. A plea for the T2W MR sequence for pituitary imaging. Pituitary 2019;22(2):195–197.
28. Potorac I, Petrossians P, Daly AF, et al. T2-weighted MRI signal predicts hormone and tumor responses to somatostatin analogs in acromegaly. Endocr Relat Cancer 2016;23(11):871–881.
29. Braileanu M, Hu R, Hoch MJ, et al. Pre-operative MRI predictors of hormonal remission status post pituitary adenoma resection. Clin Imaging 2019;55:29–34.
30. Park M, Lee SK, Choi J, et al. Differentiation between Cystic Pituitary Adenomas and Rathke Cleft Cysts: A Diagnostic Model Using MRI. AJNR Am J Neuroradiol 2015;36(10):1866–1873.
31. Grober Y, Grober H, Wintermark M, Jane JA, Oldfield EH. Comparison of MRI techniques for detecting microadenomas in Cushing's disease. J Neurosurg 2018;128(4):1051–1057.
32. Fukuhara N, Inoshita N, Yamaguchi-Okada M, et al. Outcomes of three-Tesla magnetic resonance imaging for the identification of pituitary adenoma in patients with Cushing's disease. Endocr J 2019;66(3):259–264.
33. Chatain GP, Patronas N, Smirniotopoulos JG, et al. Potential utility of FLAIR in MRI-negative Cushing's disease. J Neurosurg 2018;129(3):620–628.
34. Hardy J. Transphenoidal microsurgery of the normal and pathological pituitary. Clin Neurosurg 1969;16(CN_suppl_1):185–217.
35. Knosp E, Steiner E, Kitz K, Matula C. Pituitary adenomas with invasion of the cavernous sinus space: a magnetic resonance imaging classification compared with surgical findings. Neurosurgery 1993;33(4):610–617; discussion 617–618.
36. Hughes JD, Fattahi N, Van Gompel J, Arani A, Ehman R, Huston J 3rd. Magnetic resonance elastography detects tumoral consistency in pituitary macroadenomas. Pituitary 2016;19(3):286–292.
37. Su CQ, Zhang X, Pan T, et al. Texture Analysis of High b-Value Diffusion-Weighted Imaging for Evaluating Consistency of Pituitary Macroadenomas. J Magn Reson Imaging 2020;51(5):1507–1513.
38. Ma Z, He W, Zhao Y, et al. Predictive value of PWI for blood supply and T1-spin echo MRI for consistency of pituitary adenoma. Neuroradiology 2016;58(1):51–57.
39. Fan Y, Liu Z, Hou B, et al. Development and validation of an MRI-based radiomic signature for the preoperative prediction of treatment response in patients with invasive functional pituitary adenoma. Eur J Radiol 2019;121:108647.
40. Thompson LD, Seethala RR, Müller S. Ectopic sphenoid sinus pituitary adenoma (ESSPA) with normal anterior pituitary gland: a clinicopathologic and immunophenotypic study of 32 cases with a comprehensive review of the English literature. Head Neck Pathol 2012;6(1):75–100.
41. Ortiz E, Peldoza M, Monnier E, et al. Ectopic pituitary adenoma of the TSH-secreting sphenoidal sinus with excellent response to somatostatin analogs: theory of the embryogenesis and literature review from a clinical case. Steroids 2020;154:108535.
42. Kinoshita M, Tanaka H, Arita H, et al. Pituitary-Targeted Dynamic Contrast-Enhanced Multisection CT for Detecting MR Imaging-Occult Functional Pituitary Microadenoma. AJNR Am J Neuroradiol 2015;36(5):904–908.
43. Chun IKH, Ojumah N, Loukas M, Oskouian RJ, Tubbs RS. Martin Heinrich Rathke (1793-1860) and his pouch and cyst. Childs Nerv Syst 2018;34(3):377–379.
44. Teramoto A, Hirakawa K, Sanno N, Osamura Y. Incidental pituitary lesions in 1,000 unselected autopsy specimens. Radiology 1994;193(1):161–164.
45. Mahdi ES, Webb RL, Whitehead MT. Prevalence of pituitary cysts in children using modern magnetic resonance imaging techniques. Pediatr Radiol 2019;49(13):1781–1787.
46. Sala E, Moore JM, Amorin A, et al. Natural history of Rathke's cleft cysts: a retrospective analysis of a two centres experience. Clin Endocrinol (Oxf) 2018;89(2):178–186.
47. Han SJ, Rolston JD, Jahangiri A, Aghi MK. Rathke's cleft cysts: review of natural history and surgical outcomes. J Neurooncol 2014;117(2):197–203.
48. Wen L, Hu LB, Feng XY, et al. Rathke's cleft cyst: clinicopathological and MRI findings in 22 patients. Clin Radiol 2010;65(1):47–55.
49. Ogawa Y, Watanabe M, Tominaga T. Rathke's cleft cysts with significant squamous metaplasia: high risk of postoperative deterioration and close origins to craniopharyngioma. Acta Neurochir (Wien) 2013;155(6):1069–1075.
50. Byun WM, Kim OL, Kim D. MR imaging findings of Rathke's cleft cysts: significance of intracystic nodules. AJNR Am J Neuroradiol 2000;21(3):485–488.
51. Hofmann BM, Kreutzer J, Saeger W, et al. Nuclear beta-catenin accumulation as reliable marker for the differentiation between cystic craniopharyngiomas and Rathke cleft cysts: a clinico-pathologic approach. Am J Surg Pathol 2006;30(12):1595–1603.
52. Schweizer L, Capper D, Hölsken A, et al. BRAF V600E analysis for the differentiation of papillary craniopharyngiomas and Rathke's cleft cysts. Neuropathol Appl Neurobiol 2015;41(6):733–742.
53. Tominaga JY, Higano S, Takahashi S. Characteristics of Rathke's cleft cyst in MR imaging. Magn Reson Med Sci 2003;2(1):1–8.
54. Wang S, Nie Q, Wu Z, Zhang J, Wei L. MRI and pathological features of Rathke cleft cysts in the sellar region. Exp Ther Med 2020;19(1):611–618.
55. Wang SS, Xiao DY, Yu YH, Jing JJ, Zhao L, Wang RM. Diagnostic Significance of Intracystic Nodules on MRI in Rathke's Cleft Cyst. Int J Endocrinol 2012;2012:958732.
56. Azuma M, Khant ZA, Kitajima M, et al. Usefulness of Contrast-Enhanced 3D-FLAIR MR Imaging for Differentiating Rathke Cleft Cyst from Cystic Craniopharyngioma. AJNR Am J Neuroradiol 2020;41(1):106–110.
57. Kunii N, Abe T, Kawamo M, Tanioka D, Izumiyama H, Moritani T. Rathke's cleft cysts: differentiation from other cystic lesions in the pituitary fossa by use of single-shot fast spin-echo diffusion-weighted MR imaging. Acta Neurochir (Wien) 2007;149(8):759–769; discussion 769.
58. Choi SH, Kwon BJ, Na DG, Kim JH, Han MH, Chang KH. Pituitary adenoma, craniopharyngioma, and Rathke cleft cyst involving both intrasellar and suprasellar regions: differentiation using MRI. Clin Radiol 2007;62(5):453–462.
59. Zacharia BE, Bruce SS, Goldstein H, Malone HR, Neugut AI, Bruce JN. Incidence, treatment and survival of patients with craniopharyngioma in the Surveillance, Epidemiology and End Results program. Neuro Oncol 2012;14(8):1070–1078.
60. Larkin SJ, Ansorge O. Pathology and pathogenesis of craniopharyngiomas. Pituitary 2013;16(1):9–17.
61. Lubuulwa J, Lei T. Pathological and Topographical Classification of Craniopharyngiomas: A Literature Review. J Neurol Surg Rep 2016;77(3):e121–e127.
62. Pascual JM, Rosdolsky M, Prieto R, Straub S, Winter E, Ulrich W. Jakob Erdheim (1874-1937): father of

hypophyseal-duct tumors (craniopharyngiomas). Virchows Arch 2015;467(4):459–469.
63. Sartoretti-Schefer S, Wichmann W, Aguzzi A, Valavanis A. MR differentiation of adamantinous and squamous-papillary craniopharyngiomas. AJNR Am J Neuroradiol 1997;18(1):77–87.
64. Prabhu VC, Brown HG. The pathogenesis of craniopharyngiomas. Childs Nerv Syst 2005;21(8-9):622–627.
65. Marcus HJ, Rasul FT, Hussein Z, et al. Craniopharyngioma in children: trends from a third consecutive single-center cohort study. J Neurosurg Pediatr 2019. doi: 10.3171/2019.10.PEDS19147. Published online December 20, 2019. Accessed September 2, 2020.
66. Müller HL. The Diagnosis and Treatment of Craniopharyngioma. Neuroendocrinology 2020;110(9-10):753–766.
67. Dandurand C, Sepehry AA, Asadi Lari MH, Akagami R, Gooderham P. Adult Craniopharyngioma: Case Series, Systematic Review, and Meta-Analysis. Neurosurgery 2018;83(4):631–641.
68. Meuric S, Brauner R, Trivin C, Souberbielle JC, Zerah M, Sainte-Rose C. Influence of tumor location on the presentation and evolution of craniopharyngiomas. J Neurosurg 2005;103(5 suppl):421–426.
69. Omay SB, Chen YN, Almeida JP, et al. Do craniopharyngioma molecular signatures correlate with clinical characteristics? J Neurosurg 2018;128(5):1473–1478.
70. Kim JH, Paulus W, Heim S. BRAF V600E mutation is a useful marker for differentiating Rathke's cleft cyst with squamous metaplasia from papillary craniopharyngioma. J Neurooncol 2015;123(1):189–191.
71. Lee IH, Zan E, Bell WR, Burger PC, Sung H, Yousem DM. Craniopharyngiomas : Radiological Differentiation of Two Types. J Korean Neurosurg Soc 2016;59(5):466–470.
72. Louis DN, Perry A, Reifenberger G, et al. The 2016 World Health Organization Classification of Tumors of the Central Nervous System: a summary. Acta Neuropathol (Berl) 2016;131(6):803–820.
73. Kleinschmidt-DeMasters BK, Lopes MB. Update on hypophysitis and TTF-1 expressing sellar region masses. Brain Pathol 2013;23(5):495–514.
74. Covington MF, Chin SS, Osborn AG. Pituicytoma, spindle cell oncocytoma, and granular cell tumor: clarification and meta-analysis of the world literature since 1893. AJNR Am J Neuroradiol 2011;32(11):2067–2072.
75. Zygourakis CC, Rolston JD, Lee HS, Partow C, Kunwar S, Aghi MK. Pituicytomas and spindle cell oncocytomas: modern case series from the University of California, San Francisco. Pituitary 2015;18(1):150–158.